Neurotoxicity Research (2023) 41:16–28
https://doi.org/10.1007/s12640-022-00617-0

RESEARCH ARTICLE

CircUBE3B High Expression Participates in Sevoflurane-Induced Human Hippocampal Neuron Injury via Targeting miR-326 and Regulating MYD88 Expression

Xinye Qian[1] · Shanshan Zheng[1] · Yingfang Yu[1]

Received: 24 June 2022 / Revised: 19 September 2022 / Accepted: 5 December 2022 / Published online: 31 December 2022

Abstract

The clinical application of Sevoflurane (Sevo) brings about non-negligible neuron injury, leading to postoperative cognitive dysfunction (POCD). However, related pathogenesis is complex and not fully established. We aimed to disclose the role of circRNA UBE3B (circUBE3B) in neuron injury induced by Sevo. Cell viability and apoptosis were determined by CCK-8 and flow cytometry experiments. Inflammation production was monitored by ELISA. The expression of circUBE3B, miR-326, and myeloid differentiation factor 88 (MYD88) mRNA was assessed by quantitative real-time PCR (qPCR). Apoptosis-associated markers and MYD88 protein were quantified by western blot. The putative binding site between miR-326 and circUBE3B or MYD88 was verified by a dual-luciferase reporter experiment, and their binding was validated by a pull-down assay. Sevo treatment weakened cell viability and promoted cell apoptosis and inflammatory response. CircUBE3B expression was elevated in Sevo-treated neurons. Sevo-induced neuron injury was alleviated by circUBE3B downregulation but aggravated by circUBE3B overexpression. MiR-326 was targeted by circUBE3B, and miR-326 inhibition recovered neuron injury that was repressed by circUBE3B absence in Sevo-treated neurons. MiR-326 interacted with MYD88. MiR-326 enrichment attenuated Sevo-induced neuron injury, while these effects were reversed by MYD88 overexpression. CircUBE3B dysregulation was involved in Sevo-induced human hippocampal neuron injury via targeting the miR-326/MYD88 network.

Keywords circUBE3B · miR-326 · MYD88 · Sevoflurane · Neuron

Introduction

Sevoflurane (Sevo) is the most common inhalation anesthetic used in surgical procedures and has the advantages of fast inhalation, rapid induction, and good controllability (34,305,576) (Wang et al. 2021). However, a growing body of evidence exposes that anesthetic exposure can lead to temporary or long-term postoperative cognitive dysfunction (POCD) (Zhu et al. 2017; Fang et al. 2012; Tang et al. 2020). There is also growing concerned in the specific effects of Sevo on individuals with pre-existing cognitive impairment. Previous studies have observed that Sevo-induced neurotoxicity can lead to neurogenic inflammation, neuronal apoptosis, and abnormal protein deposition, which contribute to cognitive dysfunction (Huang et al. 2021; Xu et al. 2021; Tian et al. 2015). To date, although researchers have mentioned various mechanisms of Sevo-induced cognitive dysfunction, the exact pathophysiological changes remain unclear. Therefore, understanding the molecular mechanisms of Sevo-induced cognitive impairment is important for developing specific management strategies to improve the postoperative impact of patients.

Circular RNAs (circRNAs) are considerable modulators in multiple physiological processes (Ebbesen et al. 2017). As a class of non-coding RNA molecules, circRNAs are generated from precursor mRNA via a "back-splicing" mechanism. CircRNAs are characterized by circular structures, without 3′ and 5′ terminals, which gives rise to circRNAs high stability (Fang et al. 2019). Other non-coding RNA molecules, such as long non-coding RNA (lncRNA) and microRNA (miRNA), have been expounded to play functions in Sevo-triggered cognitive dysfunction (Hu et al. 2019; Lv et al. 2017). CircRNAs were previously

✉ Yingfang Yu
xzzqpcc@163.com

[1] Department of Anesthesiology, Fudan University Huashan Hospital, No. 12, Urumqi Road, Jing'An, Shanghai 200040, China

demonstrated to be involved in Sevo-mediated multiple biological activities, such as cancer biology (Li et al. 2020; He et al. 2020a). Besides, circRNA dysregulation was also recorded to be associated with the development of cognitive dysfunction, as well as some neurodegenerative diseases (Zhou et al. 2020; Cao et al. 2020). However, the evidence related to the involvement of circRNAs in Sevo-induced cognitive dysfunction is insufficient. The implementation of RNA sequencing identified plenty of circRNAs that were aberrantly expressed in POCD patients relative to non-POCD subjects (Gao et al. 2020a), and we noticed that circ_0028135 showed increased expression in the serum of POCD patients (Gao et al. 2020a). Circ_0028135 is produced by back-splicing from ubiquitin protein ligase E3B (UBE3B), also known as circUBE3B. Interestingly, circUBE3B expression was notably strengthened by Sevo administration in neurons in our study. We speculated that circ_0028135 was involved in Sevo-induced neuron injury.

CircRNAs participate in biology processes via diverse molecular mechanisms, such as encoding peptides, interacting with RNA-binding proteins, and acting as miRNA sponges (Zheng et al. 2019; Dong et al. 2019; Panda 2018). Abundant evidence uncovers that circRNAs may share miRNA binding sites with miRNA-targeted mRNAs and thus function as competing for endogenous RNAs (ceRNAs) (Ala 2021). To realize the regulatory mechanism of circUBE3B, we investigated the target miRNAs of circUBE3B and downstream functional mRNAs that share miRNA binding sites with circUBE3B. As a result, we observed that circUBE3B shared the same miR-326 binding site with myeloid differentiation factor 88 (MYD88), hinting that circUBE3B might function by competing with MYD88 for the miR-326 binding site. Nonetheless, the interactions among circUBE3B, miR-326, and MYD88 have not been reported.

Our work aimed to disclose the role and potential mechanism of circUBE3B in Sevo-induced neuron injury, so as to provide underlying management strategies for patients after Sevo administration. We mainly conducted gain- and loss-of-function assays to clarify the function of circUBE3B in Sevo-treated neurons. The interaction between miR-326 and circUBE3B or MYD88 was validated by the rescue experiment, thus proposing a new regulatory network of circUBE3B/miR-326/MYD88.

Materials and Methods

Cell Treatment

Human hippocampal neurons (HHNs) were directly purchased from ScienceCell Research Laboratories (San Diego, CA, USA) and cultured in a neuronal medium added with a neuronal growth supplement. Sevo (Sigma-Aldrich, St. Louis, MO, USA) was dissolved in a culture medium to prepare 1%, 2%, and 4% concentrations. HHNs were seeded in 6-well plates and treated with Sevo for 0, 12, 24, or 48 h. HHNs treated with 4% Sevo for 24 h were used in the following assays.

CCK-8 Assay

HHNs treated with different doses of Sevo were plated into 96-well plates (5000 cells/well, with 3 duplications) and subsequently cultured for different times (0, 12, 24, or 48 h). Next, cells were administered with CCK-8 (10 μL in each well) for an additional 2 h. The 450 nm absorbance of the treated cells was measured by a microplate reader (Olabo, Jinan, China) to evaluate cell viability.

Flow Cytometry Assay

The treated cells were digested with trypsin and collected for apoptosis detection using Annexin V-FITC Apoptosis Detection Kit (Sigma-Aldrich). In brief, cells were resuspended by 195 μL Annexin V-FITC buffer in 24-well plates (5×10^4 cells/well), with 3 duplicated wells for each sample. Next, 10 μL Annexin V-FITC and 5 μL propidium iodide (PI) were successively added to stain cells in the dark at room temperature. Apoptosis detection was performed using a flow cytometer (Beckman Coulter, Miami, FL, USA).

ELISA

Cell supernatant medium was collected to examine the release of inflammatory factors using commercial ELISA kits, including Human IL-1β ELISA Kit (MultiSciences, Hangzhou, China), Human IL-6 ELISA Kit (MultiSciences), and Human TNF-α ELISA Kit (MultiSciences), according to the matched guidelines.

Quantitative Real-Time PCR

Cells (1×10^6) were collected and lysed in 1 mL Trizol reagent (Sigma-Aldrich). According to the routine Trizol method, total RNA was isolated and then applied for reverse transcription using PrimeScript RT reagent Kit (Takara, Dalian, China) or HyperScript III miRNA 1st Strand cDNA Synthesis Kit (NovaBio, Shanghai, China). An equal amount of cDNA was amplified for qPCR analysis (with 3 duplications) using SYBR Green I (Takara), using the following procedures: 95 ℃ for 10 min (1 cycle), 95 ℃ for 10 s, and 60 ℃ for 1 min (40 cycles). Our study adopted β-actin (for circUBE3B and MYD88) or U6 (for miR-326) as the internal reference. The Ct value was processed using the $2^{-\Delta\Delta Ct}$ method. The primer sequences were displayed in Table 1.

Table 1 Primers sequences used for qPCR

Name		Primers for PCR (5′–3′)
circUBE3B	Forward	TTGGAATGCCTGAACAATGA
	Reverse	GAAGGTGACAAGCATCGTGA
miR-1294	Forward	GCCGAGTGTGAGGTTGGCATTG
	Reverse	CTCAACTGGTGTCGTGGA
miR-330-5p	Forward	GCCGAGTCTCTGGGCCTGTGTC
	Reverse	CTCAACTGGTGTCGTGGA
miR-326	Forward	GCCGAGCCTCTGGGCCCTTC
	Reverse	CTCAACTGGTGTCGTGGA
MYD88	Forward	ATCGTTTTATTGCTCGCCGC
	Reverse	GTGTGGATGCGATGTGATGC
GAPDH	Forward	AGAAGGCTGGGGCTCATTTG
	Reverse	AGGGGCCATCCACAGTCTTC
U6	Forward	CTTCGGCAGCACATATACT
	Reverse	AAAATATGGAACGCTTCACG

Western Blot

Utilizing RIPA reagent (Beyotime, Shanghai, China), protein samples were prepared and then quantified by BCA Protein Assay Kit (Beyotime). A total of 20 μg proteins in each well were separated by 10% SDS-PAGE and then transferred to PVDF membranes. The protein-stained membranes were subjected to QuickBlock™ Blocking Buffer for protein blocking (Beyotime). The primary and secondary antibodies were bought from Abcam (Wei et al. 2019; Chen et al. 2020a, b; Singh et al. 2022; Sun et al. 2020, 2019; Guo et al. 2018), including anti-Bax (ab32503), anti-Bcl-2 (ab32124), anti-c-caspase3 (ab2302), anti-MYD88 (ab133739), anti-β-actin (ab8227), and goat anti-rabbit IgG (ab205718). After antibody incubation, protein bands were clearly displayed using the BeyoECL Plus Kit (Beyotime), and signal density was calculated using Image J software.

Cell Transfection

A commercial pCD5-ciR expression vector was used for circUBE3B overexpression, and a circUBE3B overexpression vector was provided by Geneseed (Guangzhou, China), with a blank vector as a control. The short hairpin RNAs of circUBE3B (sh-circUBE3B) and sh-NC were also designed and synthesized by Geneseed. MiR-326 mimic (miR-326), miR-326 inhibitor (anti-miR-326), mimic control (miR-NC), and inhibitor control (anti-miR-NC) were bought from Ribobio (Guangzhou, China). A universal pcDNA vector was used for MYD88 overexpression, and the MYD88 expression vector (MYD88) was constructed by GenePharma (Shanghai, China). These oligos or vectors were introduced into the experimental cells using Lipofectamine 3000 (Invitrogen, Carlsbad, CA, USA).

Bioinformatics Tools

The public prediction tools, including starbase (http://starbase.sysu.edu.cn/) and circinteractome (https://circinteractome.nia.nih.gov/), were employed for target analysis.

Dual-Luciferase Reporter Experiment

To ensure the binding between miR-326 and circUBE3B or MYD88 3′UTR by the predicted binding sites, wild-type (WT) circUBE3B sequence fragment and MYD88 3′UTR sequence fragment containing binding sites were respectively synthesized and inserted into pmirGLO vector (Promega, Madison, WI, USA). Meanwhile, the circUBE3B sequence fragment and MYD88 3′UTR sequence fragment containing binding sites of sequence mutations (MUT) were also respectively synthesized and inserted into the pmirGLO vector. The circUBE3B-WT, circUBE3B-MUT, MYD88 3′UTR WT, and MYD88 3′UTR MUT reporter vectors were constructed and next respectively transfected with miR-326 or miR-NC into the experimental cells, culturing cells for another 48 h. Luciferase activity was analyzed using the Dual-Luciferase Reporter Assay System (Promega).

RNA Pull-Down Assay

WT, MUT probe of miR-326, and miR-NC probe were synthesized and labeled by biotin (Bio-miR-326 WT, Bio-miR-326 MUT, and Bio-miR-NC) by Ribobio. The experimental cells were infected with these probes respectively and next lysed by pull-down lysis reagent (Invitrogen). Cell lysates were subjected to Streptavidin-Dyna beads (Invitrogen). The compounds on beads were eluted from beads and then detected by qPCR.

Statistical Analysis

All assays were independently implemented three times. Data were processed using GraphPad Prism 7.0 software and finally shown as mean ± standard deviation. The Shapiro–Wilk test was used to assess the normality of data. The difference between the two groups was identified by using Student's *t*-test, and the difference in ≥ three groups was compared using analysis of variance (with Dunnett's post hoc test or Sidak's post hoc test) (Table 2). P-value < 0.05 was known as statistical significance.

Results

Sevo Induced HHN Injury and Increased the Expression of circUBE3B

In Sevo-treated HHNs, cell viability was remarkably reduced in a dose-dependent manner and also in a time-dependent manner (Fig. 1A and B). The results showed a 50% decrease

Table 2 The methods for difference comparison in different study groups

	Post hoc tests	*F* (DFn, DFd)
Figure 1A	One-way ANOVA with Dunnett's post hoc test	$F(3, 8) = 30.94$
Figure 1B	One-way ANOVA with Dunnett's post hoc test	$F(3, 8) = 42.73$
Figure 1C	Unpaired t-test	$F(2, 2) = 4.334$
Figure 1D		
IL-1β	Unpaired t-test	1.567, 2, 2
IL-6	Unpaired t-test	1.010, 2, 2
TNF-α	Unpaired t-test	2.364, 2, 2
Figure 1E	Unpaired t-test	$F(2, 2) = 10.47$
Figure 2A	Unpaired t-test	$F(2, 2) = 1.214$
Figure 2B	Welch's t-test	$F(2, 2) = 55.01$
Figure 2C	One-way ANOVA with Sidak's test post hoc test	$F(5, 12) = 36.12$
Figure 2D	One-way ANOVA with Sidak's test post hoc test	$F(5, 12) = 32.74$
Figure 2E		
Bcl-2	One-way ANOVA with Sidak's test post hoc test	$F(5, 12) = 26.46$
Bax	One-way ANOVA with Sidak's test post hoc test	$F(5, 12) = 43.05$
C-caspase3	One-way ANOVA with Sidak's test post hoc test	$F(5, 12) = 46.50$
Figure 2F		
IL-1β	One-way ANOVA with Sidak's test post hoc test	$F(5, 12) = 29.16$
IL-6	One-way ANOVA with Sidak's test post hoc test	$F(5, 12) = 33.19$
TNF-α	One-way ANOVA with Sidak's test post hoc test	$F(5, 12) = 26.48$
Figure 3B		
miR-1294	Unpaired t-test	$F(2, 2) = 1.921$
miR-330-5p	Unpaired t-test	$F(2, 2) = 5.650$
miR-326	Unpaired t-test	$F(2, 2) = 36.24$
Figure 3D	Welch's t-test	$F(2, 2) = 65.41$
Figure 3E		
circUBE3B WT	Unpaired t-test	$F(2, 2) = 1.018$
circUBE3B MUT	Unpaired t-test	$F(2, 2) = 1.333$
Figure 3F	One-way ANOVA with Dunnett's post hoc test	$F(2, 6) = 178.4$
Figure 3G	Unpaired t-test	$F(2, 2) = 1.092$
Figure 4A	Unpaired t-test	$F(2, 2) = 1.134$
Figure 4B	One-way ANOVA with Sidak's test post hoc test	$F(4, 10) = 26.07$
Figure 4D	One-way ANOVA with Sidak's test post hoc test	$F(4, 10) = 40.16$
Figure 4E		
Bcl-2	One-way ANOVA with Sidak's test post hoc test	$F(4, 10) = 22.29$
Bax	One-way ANOVA with Sidak's test post hoc test	$F(4, 10) = 32.63$
C-caspase3	One-way ANOVA with Sidak's test post hoc test	$F(4, 10) = 38.06$
Figure 4F	One-way ANOVA with Sidak's test post hoc test	$F(4, 10) = 23.84$
Figure 4G	One-way ANOVA with Sidak's test post hoc test	$F(4, 10) = 19.47$
Figure 4H	One-way ANOVA with Sidak's test post hoc test	$F(4, 10) = 22.02$
Figure 5B		
MYD88 3′UTR WT	Unpaired t-test	$F(2, 2) = 4.083$
MYD88 3′UTR MUT	Unpaired t-test	$F(2, 2) = 1.788$
Figure 5C	Unpaired t-test	$F(2, 2) = 7.348$
Figure 5D	Unpaired t-test	$F(2, 2) = 5.947$
Figure 5E	One-way ANOVA with Sidak's test post hoc test	$F(3, 8) = 120.1$
Figure 5F	One-way ANOVA with Sidak's test post hoc test	$F(3, 8) = 84.06$
Figure 6A	Unpaired t-test	$F(2, 2) = 1.974$
Figure 6B	One-way ANOVA with Sidak's test post hoc test	$F(4, 10) = 20.68$
Figure 6D	One-way ANOVA with Sidak's test post hoc test	$F(4, 10) = 27.83$
Figure 6E		

Table 2 (continued)

	Post hoc tests	*F* (DFn, DFd)
Bcl-2	One-way ANOVA with Sidak's test post hoc test	$F(4, 10) = 16.37$
Bax	One-way ANOVA with Sidak's test post hoc test	$F(4, 10) = 31.73$
C-caspase3	One-way ANOVA with Sidak's test post hoc test	$F(4, 10) = 36.96$
Figure 6F	One-way ANOVA with Sidak's test post hoc test	$F(4, 10) = 20.59$
Figure 6G	One-way ANOVA with Sidak's test post hoc test	$F(4, 10) = 30.35$
Figure 6H	One-way ANOVA with Sidak's test post hoc test	$F(4, 10) = 27.64$
Figure 7A	One-way ANOVA with Sidak's test post hoc test	$F(5, 12) = 34.93$
Figure 7B	One-way ANOVA with Sidak's test post hoc test	$F(5, 12) = 37.41$

in cell activity after treating cells with 4% Sevo for 24 h. Therefore, HHNs treated with 4% Sevo for 24 h were used in the following experiments. As a result, Sevo significantly evoked HHN apoptosis (Fig. 1C). In addition, the production of IL-1β, IL-6, and TNF-α from HHNs was greatly induced after Sevo treatment (Fig. 1D). The expression of circUBE3B was markedly elevated in Sevo-treated HHNs relative to control (Fig. 1E). The data implied that circUBE3B upregulation might be associated with Sevo-induced HHN injury.

CircUBE3B Knockdown Attenuated Sevo-Induced HHN Injury, While circUBE3B Aggravated Sevo-Induced HHN Injury

Gain- and loss-of-function experiments were conducted to analyze the function of circUBE3B in Sevo-treated HHNs. CircUBE3B expression was considerably reduced in HHNs transfected with sh-circUBE3B, while circUBE3B expression was markedly reinforced in HHNs transfected with circUBE3B (Fig. 2A and B). In function, Sevo-depleted cell viability was further inhibited by circUBE3B overexpression, while circUBE3B knockdown prevented Sevo-inhibited cell viability (Fig. 2C). CircUBE3B overexpression aggravated Sevo-induced HHN apoptosis, while circUBE3B absence relieved Sevo-induced HHN apoptosis (Fig. 2D). Sevo-reduced Bcl-2 expression was further repressed by circUBE3B upregulation, and Sevo-strengthened Bax and c-caspase3 expression was further enhanced by circUBE3B upregulation (Fig. 2E). Sevo-reduced Bcl-2 expression was restored by circUBE3B knockdown, and Sevo-enhanced Bax and c-caspase3 expression was partly repressed by circUBE3B knockdown (Fig. 2E). Moreover, Sevo-stimulated IL-1β, IL-6, and TNF-α production was further aggravated by circUBE3B forced expression, while Sevo-induced IL-1β, IL-6, and TNF-α production was largely alleviated by circUBE3B absence (Fig. 2F). The data evidenced that circUBE3B knockdown attenuated Sevo-induced HHN injury, while circUBE3B aggravated Sevo-induced HHN injury.

MiR-326 was Verified as a Target of circUBE3B

Starbase and circinteractome were utilized for the target prediction of circUBE3B. As a result, miR-1294, miR-330-5p, and miR-326 were commonly predicted by two databases (Fig. 3A). Then, we used circUBE3B probe to enrich these predicted miRNAs via pull-down assay, and only miR-326 was abundantly enriched by circUBE3B probe compared to oligo probe (Fig. 3B). The potential binding site between circUBE3B and miR-326 was displayed in Fig. 3C. Prior to dual-luciferase reporter experiment, we examined the efficiency of miR-326 mimic and found that miR-326 transfection significantly reinforced the expression of miR-326 in HHNs (Fig. 3D). Then, miR-326 enrichment remarkably weakened luciferase activity in HHNs with circUBE3B WT vector transfection (Fig. 3E). In addition, Bio-miR-326 WT probe, relative to Bio-miR-NC or Bio-miR-326 MUT, prominently enriched the expression of circUBE3B (Fig. 3F). MiR-326 expression was strikingly declined in HHNs treated with Sevo (Fig. 3G).

MiR-326 Deficiency Reversed the Functional Role of circUBE3B Knockdown

Given that miR-326 was a target of circUBE3B, we performed rescue experiments to identify whether circUBE3B played functions partly by regulating miR-326. The transfection of anti-miR-326 in HHNs notably reduced miR-326 expression (Fig. 4A). In function, cell viability was restored in Sevo-treated HHNs transfected with sh-circUBE3B, while cell viability was largely reduced in Sevo-treated HHNs transfected with sh-circUBE3B + anti-miR-326 (Fig. 4B). Besides, Sevo-induced HHN apoptosis was relieved by circUBE3B knockdown, while further miR-326 depletion partially promoted HHN apoptosis (Fig. 4C–D). CircUBE3B knockdown recovered Bcl-2 expression in Sevo-treated HHNs, while further miR-326 repression repressed Bcl-2 expression. CircUBE3B knockdown impaired Bax and c-caspase3 expression in Sevo-treated HHNs, while further miR-326 repression recovered

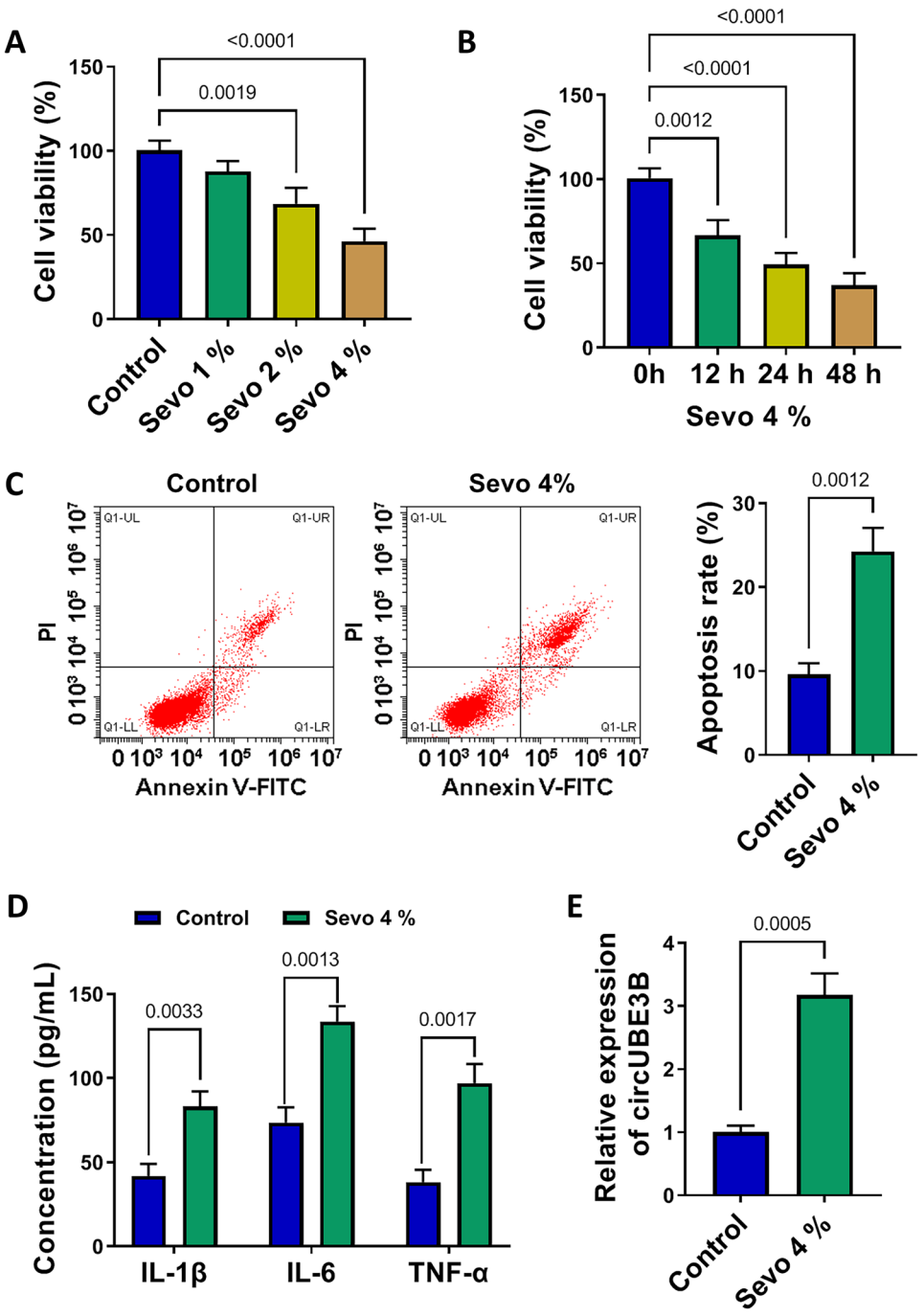

Fig. 1 Sevo induced HHN injury and promoted circUBE3B expression. **A** The viability of HHNs treated with different concentrations of Sevo was detected by CCK-8 assay (one-way ANOVA with Dunnett's post hoc test). **B** The viability of HHNs treated with 4% Sevo for different times was detected by CCK-8 assay (one-way ANOVA with Dunnett's post hoc test). **C** The apoptosis rate of HHNs treated with 4% Sevo for 24 h was checked by flow cytometry assay (unpaired t-test). **D** The release of IL-1β, IL-6, and TNF-α was examined using ELISA kits (unpaired t-test). **E** The expression of circUBE3B in Sevo-treated HHNs was measured by qPCR (unpaired t-test)

Bax and c-caspase3 expression (Fig. 4E). Additionally, the production of IL-1β, IL-6, and TNF-α was remarkably suppressed by circUBE3B knockdown in Sevo-treated HHNs, while further miR-326 inhibition recovered the production of these factors (Fig. 4F–H). The data uncovered that circUBE3B knockdown attenuated Sevo-induced HHN cell injury via regulating miR-326.

MiR-326 Targeted MYD88 3′UTR and Negatively Regulated MYD88 Expression

MiR-326 was shown to contain a binding site with MYD88 3′UTR (Fig. 5A). MiR-326 enrichment markedly diminished luciferase activity in HHNs with MYD88 3′UTR WT transfection rather than MYD88 3′UTR MUT (Fig. 5B). The

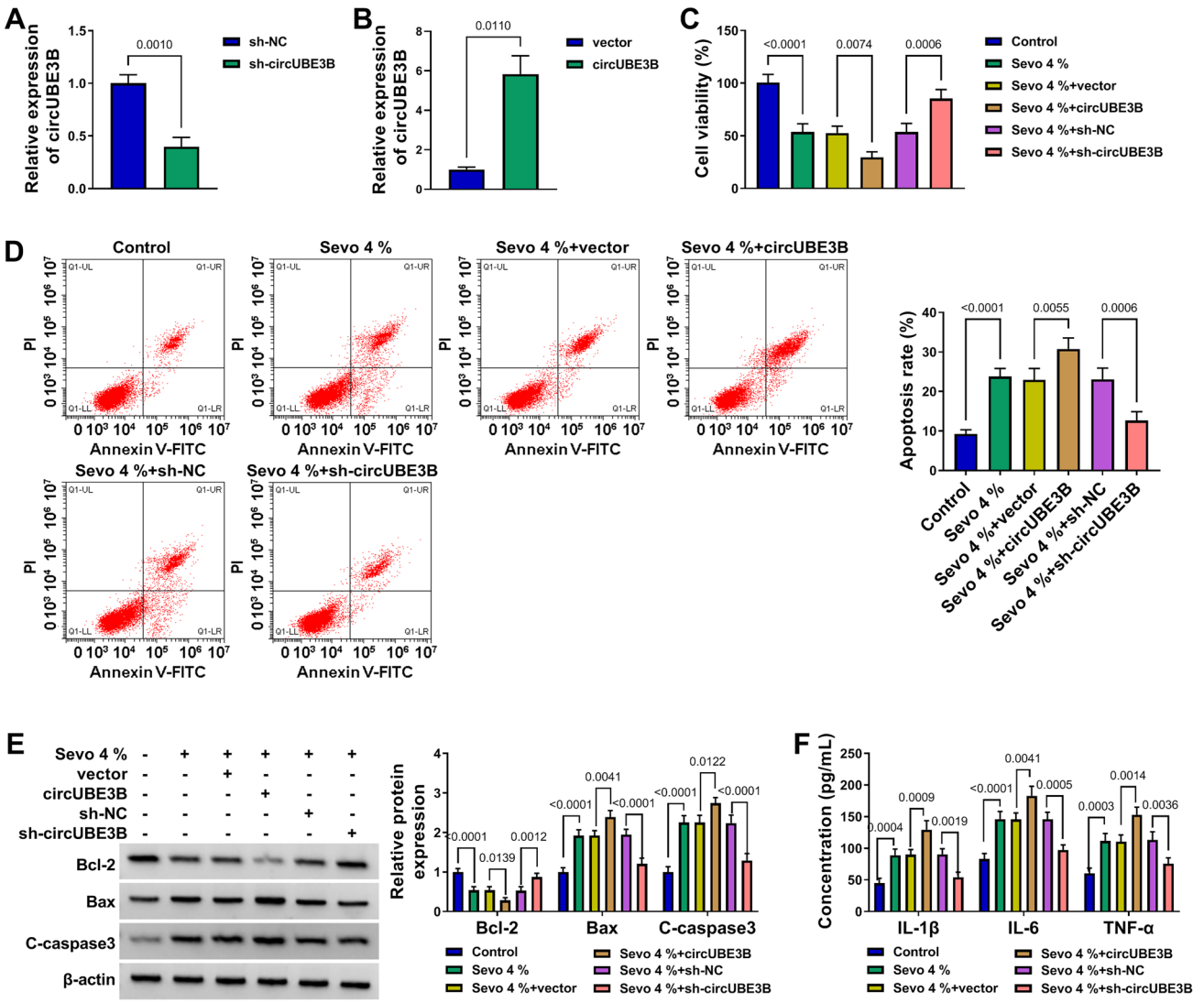

Fig. 2 Sevo-induced HHN injury was attenuated by circUBE3B knockdown. **A** CircUBE3B expression in sh-circUBE3B- or sh-NC-transfected HHNs was measured by qPCR (unpaired t-test). **B** CircUBE3B expression in circUBE3B or vector-transfected HHNs was measured by qPCR (unpaired t-test). **C** The viability of Sevo-treated HHNs after circUBE3B overexpression or knockdown was detected by CCK-8 assay (one-way ANOVA with Sidak's post hoc test). **D** The apoptosis of Sevo-treated HHNs after circUBE3B overexpression or knockdown was detected by flow cytometry assay (one-way ANOVA with Sidak's post hoc test). **E** The expression levels of Bcl-2, Bax, and C-caspase3 in Sevo-treated HHNs after circUBE3B overexpression or knockdown were measured by western blot (one-way ANOVA with Sidak's post hoc test). **F** The release of IL-1β, IL-6, and TNF-α in the culture medium of Sevo-treated HHNs after circUBE3B overexpression or knockdown was examined using ELISA kits (one-way ANOVA with Sidak's post hoc test)

expression of MYD88 was pronouncedly enhanced in Sevo-treated HHNs (Fig. 5C and D). Moreover, MYD88 expression was considerably decreased in HHNs after miR-326 enrichment, while its expression was markedly reinforced in HHNs after miR-326 inhibition (Fig. 5E and F). The data verified that miR-326 negatively modulated MYD88 expression.

MYD88 Overexpression Reversed the Functional Effects of miR-326

The transfection of the MYD88 expression vector prominently strengthened MYD88 expression in HHNs (Fig. 6A). In function, Sevo-depleted cell viability was largely recovered by

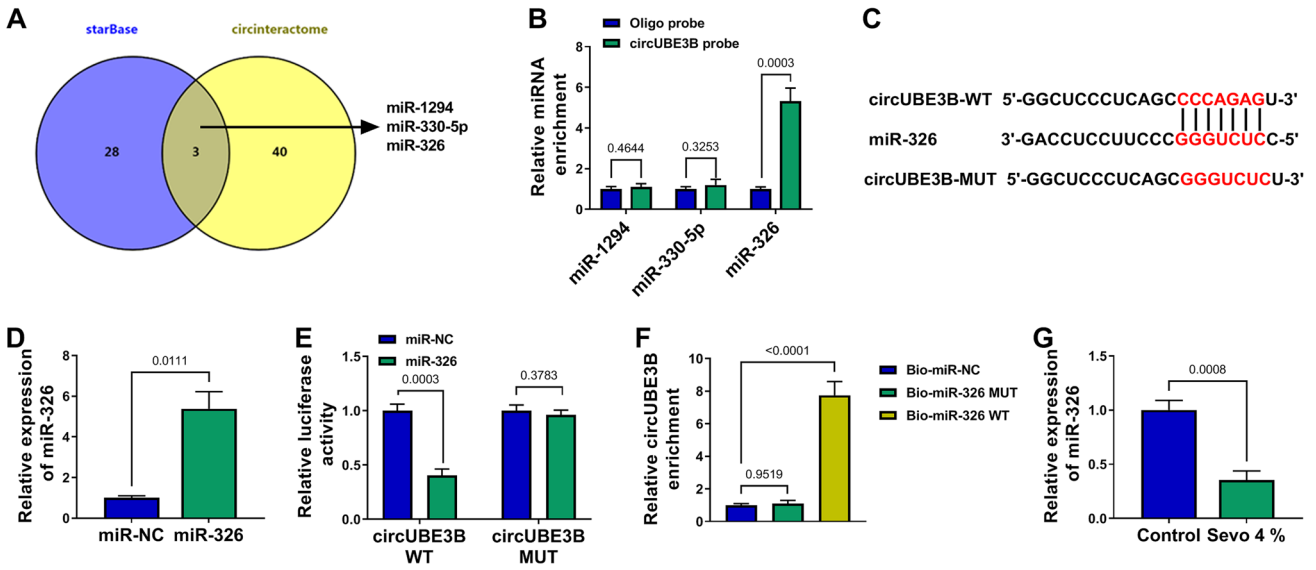

Fig. 3 MiR-326 was characterized as a target of circUBE3B. **A** Starbase and circinteractome were used to predict the target miRNAs of circUBE3B. **B** The predicted miRNAs were screened using a circUBE3B probe by pull-down assay (unpaired t-test). **C** The WT and MUT sequence fragment of circUBE3B used in dual-luciferase reporter analysis. **D** The efficiency of the miR-326 mimic was checked by qPCR (unpaired t-test). **E** The binding site between circUBE3B and miR-326 was validated by dual-luciferase reporter analysis (unpaired t-test). **F** The binding between circUBE3B and miR-326 was verified by pull-down assay (one-way ANOVA with Dunnett's post hoc test). **G** MiR-326 expression in Sevo-treated HHNs was measured by qPCR (unpaired t-test)

miR-326 enrichment, while MYD88 overexpression partially repressed miR-326-recovered cell viability (Fig. 6B). Meanwhile, we detected that Sevo-depleted cell viability was further repressed by miR-326 inhibitor or MYD88 overexpression (Fig. S1). Sevo-induced cell apoptosis was largely attenuated by miR-326 enrichment, while MYD88 overexpression partially recovered miR-326-suppressed cell apoptosis (Fig. 6C and D). Additionally, Bcl-2 expression in Sevo-treated HHNs was restored by miR-326 transfection but largely repressed by miR-326 + MYD88 transfection, while Bax and c-caspase3 expression in Sevo-treated HHNs was repressed by miR-326 transfection but largely promoted by miR-326 + MYD88 transfection (Fig. 6E). The release of IL-1β, IL-6, and TNF-α stimulated by Sevo was remarkably repressed by mir-326 enrichment, while additional MYD88 overexpression recovered the release of these factors (Fig. 6F–H). Overall, miR-326 enrichment alleviated Sevo-induced HHN cell injury via regulating MYD88.

CircUBE3B Knockdown Inhibited MYD88 Expression by Upregulating miR-326

We additionally monitored that MYD88 expression was pronouncedly repressed in Sevo-treated HHNs after sh-circUBE3B transfection, while its expression was considerably restored in Sevo-treated HHNs after sh-circUBE3B + anti-miR-326 transfection (Fig. 7A and B), indicating that circUBE3B positively regulated MYD88 expression via targeting miR-326.

Discussion

Our current study determined that circUBE3B was highly expressed in Sevo-treated HHNs. Sevo evoked HHN injury via impairing cell viability and enhancing cell apoptosis and inflammation production, while the injury was alleviated by circUBE3B knockdown. Mechanically, circUBE3B competed for the miR-326 binding site with the MYD88 3′UTR, and circUBE3B thereby positively regulated MYD88 expression via targeting miR-326. Rescue experiments confirmed their interactions in Sevo-induced HNN injury, manifesting that circUBE3B contributed to Sevo-induced neuron injury via governing the miR-326/MYD88 network.

Due to the common application of Sevo in clinical anesthesia, adverse reactions caused by Sevo exposure are of concern. The production of inflammation factors, neuron apoptotic rate, and oxidative stress was strikingly strengthened in the hippocampal region of brain tissues from Sevo-administered mice (Gao et al. 2020b). Besides, dendritic length, branch amount, and dendritic spine density were greatly decreased in pyramidal neurons of Sevo-administered rats (Liao et al. 2021). It was also evidenced that Sevo induced autophagy impairment in hippocampal neurons of aged rats (Zhang et al.

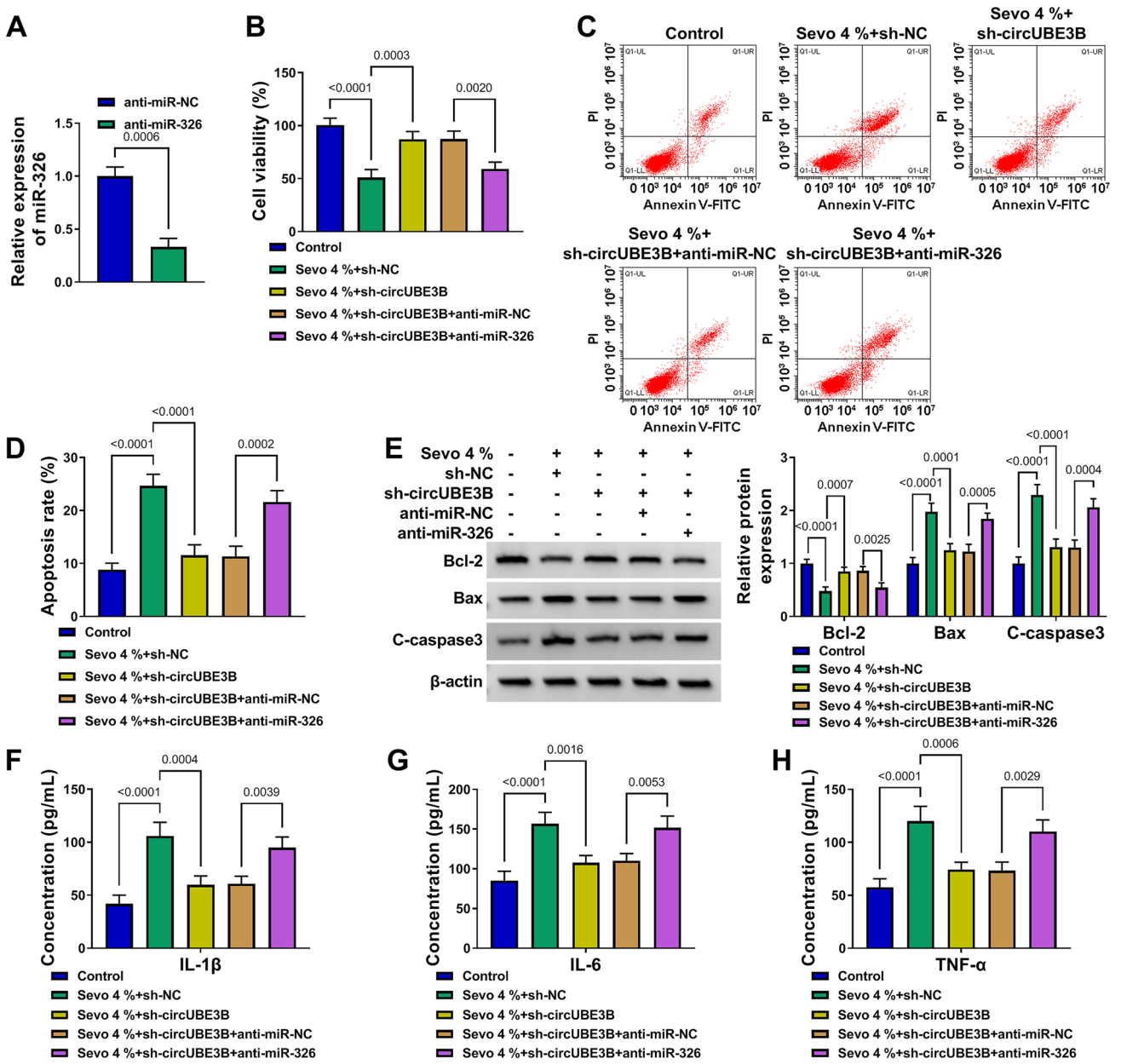

Fig. 4 CircUBE3B knockdown attenuated Sevo-induced HHN injury via upregulating miR-326. **A** The efficiency of anti-miR-326 was checked by qPCR (unpaired t-test). (B-H) In Sevo-treated HHNs transfected with sh-circUBE3B or sh-circUBE3B + anti-miR-326, **B** cell viability was checked by CCK-8 assay (one-way ANOVA with Sidak's post hoc test). **C** and **D** Cell apoptosis was examined using flow cytometry assay (one-way ANOVA with Sidak's post hoc test). **E** The expression levels of Bcl-2, Bax, and C-caspase3 were measured by western blot assay (one-way ANOVA with Sidak's post hoc test). **F**–**H** The release of IL-1β, IL-6, and TNF-α was investigated using ELISA kits (one-way ANOVA with Sidak's post hoc test)

2016a; Chen et al. 2020c). Consistent with these views, we unveiled that Sevo depleted neuron viability in a dose- and time-dependent manner and promoted neuroapoptosis and inflammation production. After realizing the effects of Sevo on neurons, molecular mechanisms regarding Sevo-induced neuron injury have been addressed in emerging studies. For example, miR-188-3p was overexpressed by Sevo in neurons, and miR-188-3p targeting the MDM2 gene was responsible for Sevo-caused neuron apoptosis (Wang et al. 2018). Besides, Sevo-induced neuronal apoptosis might be associated with the decrease of PI3K/Akt signaling activity (Ma et al. 2016). The decrease of lncRNA Gm15621 expression was observed in Sevo-treated hippocampal neurons, and Sevo-induced cell apoptosis and inflammation were partly attributed to the loss of Gm15621 (Zhao and Ai 2020). We for the first time introduced the dysregulation of circRNA in Sevo-induced neurons

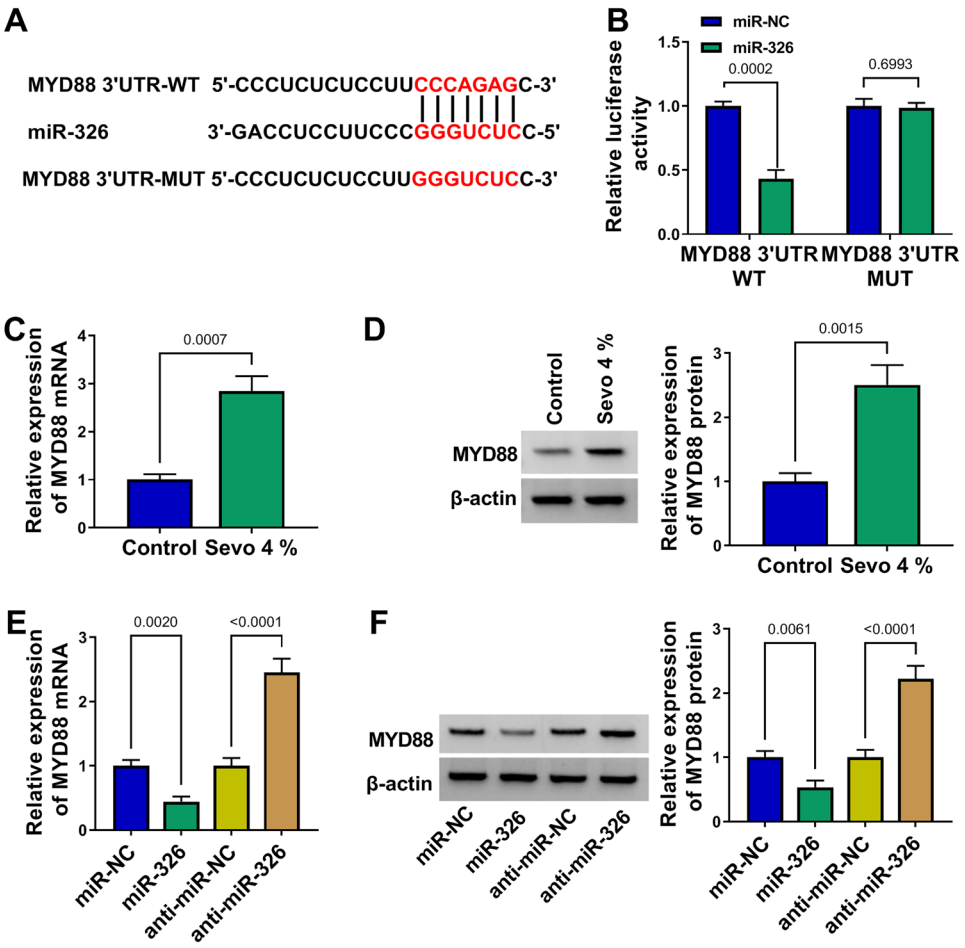

Fig. 5 MiR-326 targeted MYD88. **A** and **B** The predicted binding site between miR-326 and MYD88 3′UTR by starbase was verified by dual-luciferase reporter assay (unpaired t-test). **C** and **D** The expression of MYD88 in Sevo-treated HHNs was checked by qPCR and western blot (unpaired t-test). **E** and **F** The expression of MYD88 in HHNs after miR-326 enrichment or inhibition was checked by qPCR and western blot (one-way ANOVA with Sidak's post hoc test)

and discovered that circUBE3B expression was pronouncedly strengthened by Sevo in HHNs (Gao et al. 2020a). CircUBE3B was originally shown to be highly regulated in the serum of POCD patients, hinting that circUBE3B overexpression might be linked to POCD development. In our analysis, circUBE3B knockdown largely alleviated Sevo-induced HNN dysfunction, while circUBE3B reintroduction enhanced Sevo-induced HNN dysfunction. Our data demonstrated that circUBE3B's high expression was associated with Sevo-induced neuron injury. The targeted inhibition of circUBE3B had the potency to improve Sevo-induced neuron injury, which may be used as a promising strategy to treat Sevo-caused cognitive dysfunction.

In view of the sponge-like effects of circRNA on miRNAs, we identified the target miRNAs of circUBE3B. Among the predicted miRNAs, miR-326 aroused our interest.

MiR-326 played neuroprotective effects to prevent neuron apoptosis and pyroptosis in some neurodegenerative diseases (He et al. 2020b; Zhang et al. 2021). Besides, miR-326 was involved in Sevo-inhibited lung cancer carcinogenesis, and Sevo inhibited lung cancer cell growth and triggered apoptosis via enhancing miR-326 expression (Su et al. 2020). MiR-326 was screened as a target of circUBE3B in our study due to the involvement of miR-326 in neuron injury and Sevo function. We discovered that miR-326 expression was greatly reduced in Sevo-treated HHNs. Functionally, the depletion of miR-326 attenuated the neuroprotective effects of circUBE3B knockdown in Sevo-treated HHNs, while miR-326 enrichment in Sevo-treated HHNs alleviated Sevo-induced HNN viability impairment, apoptosis, and inflammation. The data indicated that circUBE3B contributed to Sevo-induced neuron injury via mediating miR-326.

Considering that circUBE3B might function as a ceRNA to compete for the miR-326 binding site with downstream mRNAs, we explored the targets of miR-326. Interestingly, we discovered that circUBE3B shared the same miR-326 binding site with MYD88 3′UTR. Our results also exposed that MYD88 expression was remarkably downregulated in neurons with sh-circUBE3B transfection, while its expression was largely restored in neurons with sh-circUBE3B + anti-miR-326 transfection, suggesting that circUBE3B positively regulated MYD88 expression via targeting miR-326. MYD88, a TLR signaling adaptor protein, played a vital role in the inflammation response after neuron injury (Li et al. 2013; Liu et al. 2016), and MYD88 inhibition exerted neuroprotection effects in mice with traumatic brain injury (Zhang et al. 2016b). In addition, MYD88 downregulation attenuated

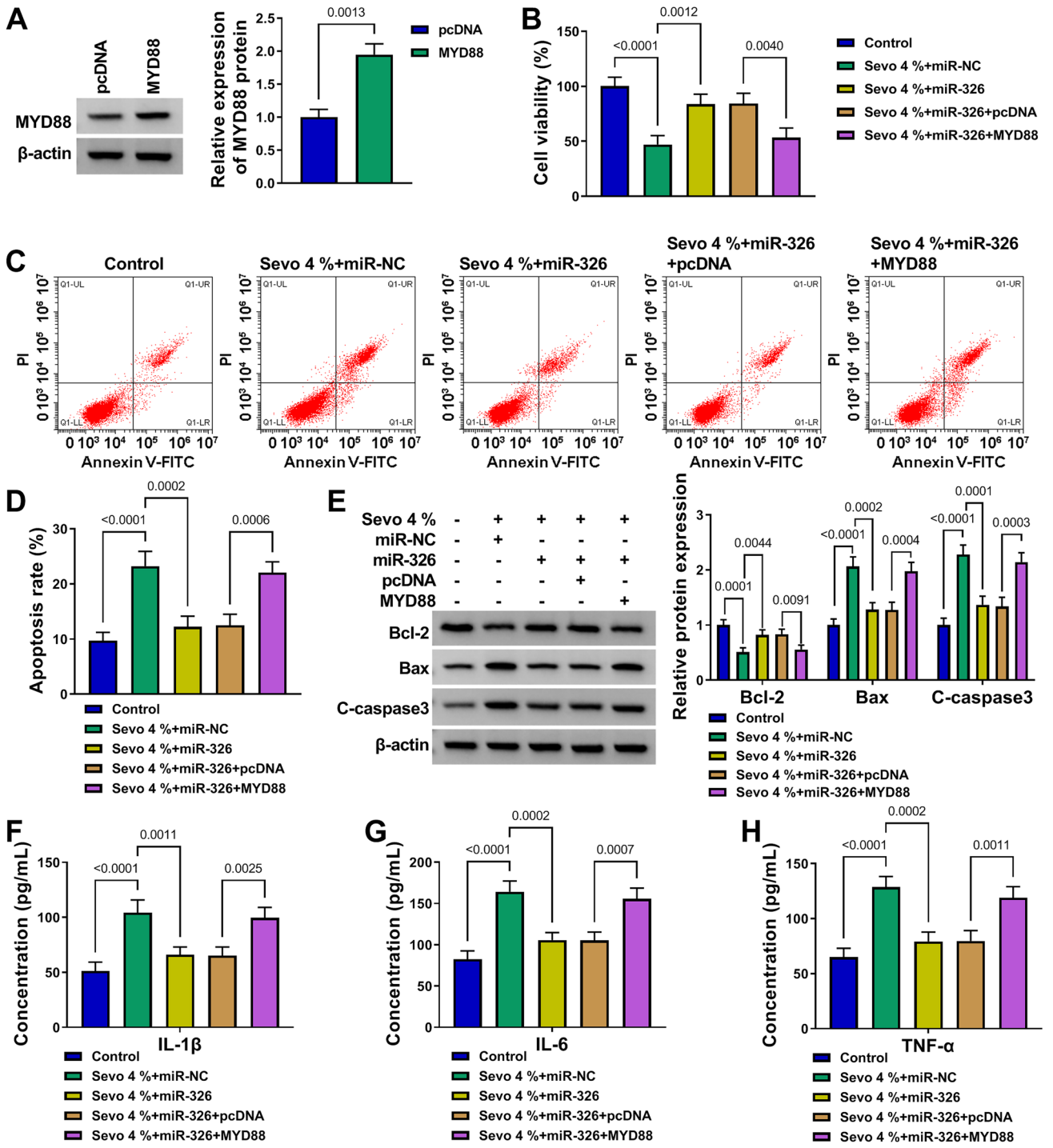

Fig. 6 MiR-326 enrichment attenuated Sevo-induced HHN injury via suppressing MYD88. **A** The efficiency of MYD88 overexpression vector was checked by western blot (unpaired t-test). **B**–**H** In Sevo-treated HHNs transfected with miR-326 or miR-326 + MYD88, **B** cell viability was examined using CCK-8 assay (one-way ANOVA with Sidak's post hoc test). **C** and **D** Cell apoptosis was examined using flow cytometry assay (one-way ANOVA with Sidak's post hoc test). **E** The expression levels of Bcl-2, Bax, and C-caspase3 were measured by western blot (one-way ANOVA with Sidak's post hoc test). **F**–**H** The release of IL-1β, IL-6, and TNF-α was investigated using ELISA kits (one-way ANOVA with Sidak's post hoc test)

neuropathic pain via reducing the release of inflammatory factors (Liu et al. 2017). Moreover, MYD88 expression was strikingly enhanced in brain tissues of aged rats administered with Sevo, and high MYD88 expression was involved in Sevo-induced inflammation responses (Li et al. 2019). Consistent with these findings, we also observed the upregulation

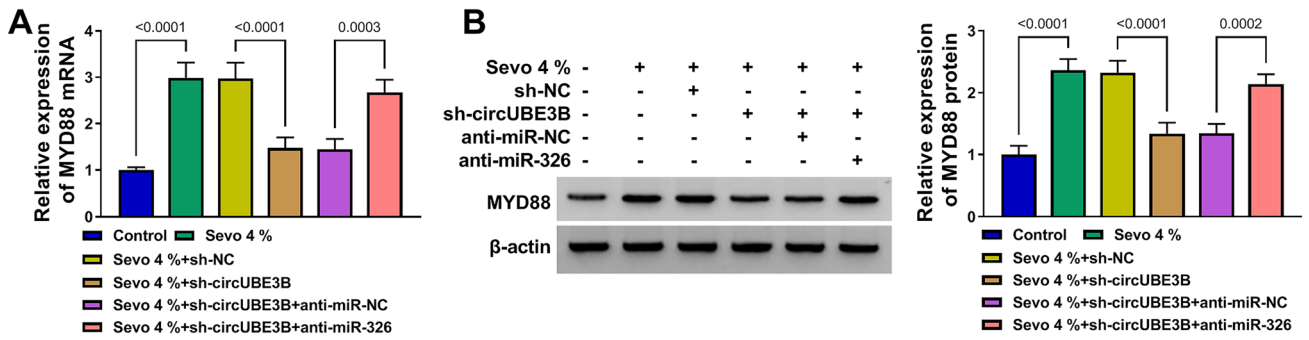

Fig. 7 CircUBE3B positively regulated MYD88 expression via targeting miR-326. **A** and **B** The expression of MYD88 in Sevo-treated HHNs with sh-circUBE3B transfection or sh-circUBE3B + anti-miR-326 transfection was measured by qPCR and western blot assays (one-way ANOVA with Sidak's post hoc test)

of MYD88 in Sevo-administered HHNs. In function, MYD88 overexpression partly abolished the neuroprotection effects of miR-326 in Sevo-treated HHNs, thus recovering Sevo-induced HHN viability impairment, apoptosis, and inflammation production. Our data verified that MYD88 contributed to Sevo-induced neuron injury, and miR-326 targeted MYD88 to suppress MYD88 function.

However, this study was only elaborated from the perspective of in vitro assays. In the next step, we will use circUBE3B lentivirus vector or circUBE3B specific inhibitors in animals to explore the effects of sevoflurane on neuron cells and the role of sevoflurane in the mechanism of long-term learning and memory disorders in animal models.

Conclusion

Collectively, we for the first time identified that circUBE3B expression was reinforced in Sevo-treated HHNs, and circUBE3B contributed to Sevo-induced HHN apoptosis and inflammation. CircUBE3B participated in Sevo-induced neuron injury via mediating the miR-326/MYD88 network.

Supplementary Information The online version contains supplementary material available at https://doi.org/10.1007/s12640-022-00617-0.

Author Contribution Xinye Qian designed and performed the research; Shanshan Zheng and Yingfang Yu analyzed the data; Xinye Qian wrote the manuscript. All authors read and approved the final manuscript.

Availability of Data and Materials Not applicable.

Declarations

Ethics Approval and Consent to Participate Not applicable.

Consent for Publication Not applicable.

Competing Interests The authors declare no competing interests.

References

Ala U (2021) Competing endogenous RNAs and cancer: how coding and non-coding molecules cross-talk can impinge on disease. Int J Biochem Cell Biol 130:105874

Cao C, Deng F, Hu Y (2020) Dexmedetomidine alleviates postoperative cognitive dysfunction through circular RNA in aged rats. 3 Biotech 10:176

Chen J, Xia D, Xu M, Su R, Lin W, Guo D et al (2020a) Expression and significance of MyD88 in patients with gastric cardia cancer in a high-incidence area of China. Front Oncol 10:559

Chen X, Yao Z, Peng X, Wu L, Wu H, Ou Y et al (2020b) Eupafolin alleviates cerebral ischemia/reperfusion injury in rats via blocking the TLR4/NFkappaB signaling pathway. Mol Med Rep 22:5135–5144

Chen Y, Zhang P, Lin X, Zhang H, Miao J, Zhou Y et al (2020c) Mitophagy impairment is involved in sevoflurane-induced cognitive dysfunction in aged rats. Aging (albany NY) 12:17235–17256

Dong W, Dai ZH, Liu FC, Guo XG, Ge CM, Ding J et al (2019) The RNA-binding protein RBM3 promotes cell proliferation in hepatocellular carcinoma by regulating circular RNA SCD-circRNA 2 production. EBioMedicine 45:155–167

Ebbesen KK, Hansen TB, Kjems J (2017) Insights into circular RNA biology. RNA Biol 14:1035–1045

Fang F, Xue Z, Cang J (2012) Sevoflurane exposure in 7-day-old rats affects neurogenesis, neurodegeneration and neurocognitive function. Neurosci Bull 28:499–508

Fang S, Pan J, Zhou C, Tian H, He J, Shen W et al (2019) Circular RNAs serve as novel biomarkers and therapeutic targets in cancers. Curr Gene Ther 19:125–133

Gao R, Chen C, Zhao Q, Li M, Wang Q, Zhou L et al (2020a) Identification of the potential key circular RNAs in elderly patients with postoperative cognitive dysfunction. Front Aging Neurosci 12:165

Gao Y, Ma L, Han T, Wang M, Zhang D, Wang Y (2020b) Protective role of protocatechuic acid in sevoflurane-induced neuron apoptosis, inflammation and oxidative stress in mice. Restor Neurol Neurosci 38:323–331

Guo XQ, Cao YL, Zhao L, Zhang X, Yan ZR, Chen WM (2018) p38 mitogen-activated protein kinase gene silencing rescues rat hippocampal neurons from ketamine-induced apoptosis: an in vitro study. Int J Mol Med 42:1401–1410

He J, Zhao H, Liu X, Wang D, Wang Y, Ai Y et al (2020a) Sevoflurane suppresses cell viability and invasion and promotes cell apoptosis in colon cancer by modulating exosomemediated circHMGCS1 via the miR34a5p/SGPP1 axis. Oncol Rep 44:2429–2442

He B, Chen W, Zeng J, Tong W, Zheng P (2020b) MicroRNA-326 decreases tau phosphorylation and neuron apoptosis through inhibition of the JNK signaling pathway by targeting VAV1 in Alzheimer's disease. J Cell Physiol 235:480–493

Hu X, Hu X, Huang G (2019) LncRNA MALAT1 is involved in sevoflurane-induced neurotoxicity in developing rats. J Cell Biochem 120: 18209–18218

Huang X, Ying J, Yang D, Fang P, Wang X, Zhou B et al (2021) The mechanisms of sevoflurane-induced neuroinflammation. Front Aging Neurosci 13:717745

Li W, Ling HP, You WC, Ji XJ, Tang Y, Zhao JB et al (2013) Recombinant high-mobility group box 1 protein (HMGB-1) promotes myeloid differentiation primary response protein 88 (Myd88) upregulation in mouse primary cortical neurons. Neurol Sci 34:847–853

Li Y, Liu L, Tian Y, Zhang J (2019) Rapamycin improves sevofluraneinduced cognitive dysfunction in aged rats by mediating autophagy through the TLR4/MyD88/NFkappaB signaling pathway. Mol Med Rep 20:3085–3094

Li H, Xia T, Guan Y, Yu Y (2020) Sevoflurane regulates glioma progression by Circ_0002755/miR-628-5p/MAGT1 Axis. Cancer Manag Res 12:5085–5098

Liao Z, Huang Z, Li J, Li H, Miao L, Liu Y et al (2021) Regulation of CRMP2 by Cdk5 and GSK-3beta participates in sevoflurane-induced dendritic development abnormalities and cognitive dysfunction in developing rats. Toxicol Lett 341:68–79

Liu XJ, Liu T, Chen G, Wang B, Yu XL, Yin C et al (2016) TLR signaling adaptor protein MyD88 in primary sensory neurons contributes to persistent inflammatory and neuropathic pain and neuroinflammation. Sci Rep 6:28188

Liu F, Wang Z, Qiu Y, Wei M, Li C, Xie Y et al (2017) Suppression of MyD88-dependent signaling alleviates neuropathic pain induced by peripheral nerve injury in the rat. J Neuroinflammation 14:70

Lv X, Yan J, Jiang J, Zhou X, Lu Y, Jiang H (2017) MicroRNA-27a-3p suppression of peroxisome proliferator-activated receptor-gamma contributes to cognitive impairments resulting from sevoflurane treatment. J Neurochem 143:306–319

Ma R, Wang X, Peng P, Xiong J, Dong H, Wang L et al (2016) Alpha-Lipoic acid inhibits sevoflurane-induced neuronal apoptosis through PI3K/Akt signalling pathway. Cell Biochem Funct 34:42–47

Panda AC (2018) Circular RNAs act as miRNA sponges. Adv Exp Med Biol 1087:67–79

Singh T, Beatty A, Peterson JR (2022) The AMPK-related kinase NUAK2 suppresses glutathione peroxidase 4 expression and promotes ferroptotic cell death in breast cancer cells. Cell Death Discov 8:253

Su G, Yan Z, Deng M (2020) Sevoflurane inhibits proliferation, invasion, but enhances apoptosis of lung cancer cells by Wnt/beta-catenin signaling via regulating lncRNA PCAT6/miR-326 Axis. Open Life Sci 15:159–172

Sun XH, Song MF, Song HD, Wang YW, Luo MJ, Yin LM (2019) miR155 mediates inflammatory injury of hippocampal neuronal cells via the activation of microglia. Mol Med Rep 19:2627–2635

Sun W, Zhao J, Li C (2020) Dexmedetomidine provides protection against hippocampal neuron apoptosis and cognitive impairment in mice with Alzheimer's disease by mediating the miR-129/YAP1/JAG1 Axis. Mol Neurobiol 57:5044–5055

Tang X, Zhao Y, Zhou Z, Yan J, Zhou B, Chi X et al (2020) Resveratrol mitigates sevoflurane-induced neurotoxicity by the SIRT1-dependent regulation of BDNF expression in developing mice. Oxid Med Cell Longev 2020:9018624

Tian Y, Guo S, Wu X, Ma L, Zhao X (2015) Minocycline alleviates sevoflurane-induced cognitive impairment in aged rats. Cell Mol Neurobiol 35:585–594

Wang L, Zheng M, Wu S, Niu Z (2018) MicroRNA-188-3p is involved in sevoflurane anesthesia-induced neuroapoptosis by targeting MDM2. Mol Med Rep 17:4229–4236

Wang CM, Chen WC, Zhang Y, Lin S, He HF (2021) Update on the mechanism and treatment of sevoflurane-induced postoperative cognitive dysfunction. Front Aging Neurosci 13:702231

Wei W, Huo B, Shi X (2019) miR-600 inhibits lung cancer via down-regulating the expression of METTL3. Cancer Manag Res 11: 1177–1187

Xu R, Zhu Y, Jia J, Li WX, Lu Y (2021) RIPK1/RIPK3-mediated necroptosis is involved in sevoflurane-induced neonatal neurotoxicity in the rat hippocampus. Cell Mol Neurobiol

Zhang X, Zhou Y, Xu M, Chen G (2016a) Autophagy is involved in the sevoflurane anesthesia-induced cognitive dysfunction of aged rats. PLoS ONE 11:e0153505

Zhang HS, Li H, Zhang DD, Yan HY, Zhang ZH, Zhou CH et al (2016b) Inhibition of myeloid differentiation factor 88(MyD88) by ST2825 provides neuroprotection after experimental traumatic brain injury in mice. Brain Res 1643:130–139

Zhang Q, Huang XM, Liao JX, Dong YK, Zhu JL, He CC et al (2021) LncRNA HOTAIR promotes neuronal damage through facilitating NLRP3 mediated-pyroptosis activation in Parkinson's disease via regulation of miR-326/ELAVL1 Axis. Cell Mol Neurobiol 41:1773–1786

Zhao Y, Ai Y (2020) Overexpression of lncRNA Gm15621 alleviates apoptosis and inflammation response resulting from sevoflurane treatment through inhibiting miR-133a/Sox4. J Cell Physiol 235:957–965

Zheng X, Chen L, Zhou Y, Wang Q, Zheng Z, Xu B et al (2019) A novel protein encoded by a circular RNA circPPP1R12A promotes tumor pathogenesis and metastasis of colon cancer via Hippo-YAP signaling. Mol Cancer 18:47

Zhou H, Li F, Ye W, Wang M, Zhou X, Feng J et al (2020) Correlation between plasma CircRNA-089763 and postoperative cognitive dysfunction in elderly patients undergoing non-cardiac surgery. Front Behav Neurosci 14:587715

Zhu G, Tao L, Wang R, Xue Y, Wang X, Yang S et al (2017) Endoplasmic reticulum stress mediates distinct impacts of sevoflurane on different subfields of immature hippocampus. J Neurochem 142:272–285